First-principles study of a pressure-induced spin transition in multiferroic Bi_2FeCrO_6

Marco Goffinet,[1] Jorge Íñiguez,[2] and Philippe Ghosez[1]
[1]*Physique Théorique des Matériaux, Université de Liège, B-5, 4000 Sart-Tilman, Belgium*
[2]*Institut de Ciència de Materials de Barcelona (ICMAB-CSIC), Campus UAB, 08193 Bellaterra, Spain*
(Received 26 February 2010; revised manuscript received 12 May 2012; published 12 July 2012)

We report on a first-principles study of the structural, electronic, and magnetic properties of multiferroic double perovskite Bi_2FeCrO_6, using density functional theory within the local spin-density approximation (LSDA), the LSDA + U approximation as well as a hybrid functional scheme. We show that Bi_2FeCrO_6 presents two competing ferrimagnetic phases, sharing the same total magnetic moment of $2\mu_B$ per unit cell but with a different electronic configuration for the Fe^{3+} species. The phase with high-spin iron is the ground state at ambient conditions, but we predict that low-spin iron gets stabilized under compression. We also investigate the corresponding ferromagnetic phases, and show that the magnetic couplings sharply decrease when moving form high- to low-spin Fe^{3+}.

DOI: 10.1103/PhysRevB.86.024415 PACS number(s): 75.40.Mg, 75.85.+t, 64.70.−p

I. INTRODUCTION

Multiferroic materials combining electric and magnetic orderings within the same phase have attracted increasing interest during recent years. Bismuth ferrite, $BiFeO_3$, which presents at room temperature ferroelectric (FE) and nearly *G*-type antiferromagnetic (AFM) orders, is one of the most extensively studied compounds of this kind. $BiFeO_3$ exhibits a *R3c* rhombohedral ground state that consists of a distorted perovskite structure with a ten-atom unit cell, and can be seen as an end member of a more general family of potentially multiferroic double-perovskites $Bi_2MM'O_6$.

Antiferromagnetism in $BiFeO_3$ arises from the opposite spin of the two rocksalt ordered Fe sublattices. In $Bi_2MM'O_6$ compounds such as Bi_2FeCrO_6, where the two sublattices are occupied by distinct transition metal ions ($M \neq M'$), one might expect "*G*-type ferrimagnetism" leading to a nonzero magnetization, and thus to even more attractive applications. Bi_2FeCrO_6 has been successfully grown in thin-film form, and its multiferroic character was experimentally demonstrated.[1,2] Previously, this was predicted by Baettig *et al.*, who theoretically analyzed the ferroelectric and magnetic properties of Bi_2FeCrO_6, as well as its crystallographic and electronic structures.[3,4] According to their LSDA + U calculations, the ground state structure of this compound is insulating with *R3* symmetry and exhibits simultaneously ferroelectric and ferrimagnetic orders, with both Cr^{3+} and Fe^{3+} in a high-spin configuration (FiMHS). In contrast, within the LSDA they found a halfmetallic ferrimagnetic ground state with Fe^{3+} in a low-spin configuration (FiMLS-Fe), and interpreted this unexpected result as a failure of the LSDA.

In $BiFeO_3$, recent first-principles calculations[5] have highlighted a transition from a high-spin (HS) to a low-spin (LS) phase under isotropic pressure at about 40 GPa, in agreement with experimental data.[6] One may thus wonder whether such a competition between HS and LS states is specific to $BiFeO_3$ or is a general feature of $Bi_2MM'O_6$ compounds containing Fe or other species susceptible of presenting such a behavior (e.g., Co). Note that there are good reasons to expect such a spin crossover will occur in other compounds, as it originates from a competition between Hund's couplings and crystal-field splittings that is rather commonly found among oxides.[7]

Here, we reinvestigate the structural, electronic, and magnetic properties of Bi_2FeCrO_6 from first-principles using different theoretical schemes. We highlight, within all of our functionals, the existence of stable FiMHS-Fe and FiMLS-Fe phases and predict a FiMHS-Fe to FiMLS-Fe transition under compressive pressure. We have also investigated the relative stability of the corresponding ferromagnetic phases (FMHS and FMLS).

II. TECHNICAL DETAILS

We worked within density functional theory (DFT). Most of our calculations were performed with the Vienna *ab initio* simulation package (VASP),[8–10] using the projector augmented plane-wave (PAW) method. We worked within the local-spin-density approximation (LSDA), both with and without the so-called LSDA + U correction for a better description of Fe and Cr 3*d* electrons. We considered both the formulation of Dudarev *et al.*[11] with $U_{\text{eff}} = 2$ eV and that of Anisimov *et al.*[12] with $U = 3$ eV and $J = 0.8$ eV as done in Ref. 3. Bi's $5d^{10}6s^26p^3$, Fe's $3p^63d^64s^2$, Cr's $3p^63d^54s^1$, and O's $2s^22p^4$ electrons were treated as valence. An $8 \times 8 \times 8$ Monkhorst-Pack grid of *k* points and a 500 eV plane-wave energy cutoff were used. Electronic self-consistence cycles were converged down to 10^{-8} eV, and the structure relaxed until the residual forces were lower than 10^{-2} eV/Å. For density of states (DOS) calculations, the Monkhorst-Pack grid was increased to $16 \times 16 \times 16$.

As the class of $Bi_2MM'O_6$ compounds contains two nonequivalent transition-metal sites, the choice of the LSDA + U formulation and of the corresponding parameters is particularly delicate. In an attempt to circumvent this difficulty, we also performed calculations using the recently proposed B1-WC hybrid functional which combines Wu-Cohen generalized gradient approximation (GGA) exchange, Perdew-Burke-Ernzerhof (PBE) correlation, and 16% of exact exchange as further detailed in Ref. 13. This functional was successfully applied to $BiFeO_3$,[14] suggesting that it can similarly provide reliable structural and electronic properties in Bi_2FeCrO_6. The hybrid calculations were performed using the CRYSTAL06 package.[15] The all-electron Gaussian basis sets used for the Fe, Cr, and O atoms are described, respectively, in Refs. 16, 17, and 18. For the Bi atoms, we used the built-in

Hay-Wadt large-core pseudopotential and the associated basis set given in Ref. 19. The self-consistent field calculations were converged down to 2.7×10^{-7} eV and the structure relaxed until the residual forces were lower than 5.1×10^{-4} eV/Å.

III. RESULTS

A. Structure and magnetic moment

First, relaxations of Bi_2FeCrO_6 have been performed using the LSDA, LSDA + U (with $U = 3$ eV and $J = 0.8$ eV and with $U_{\text{eff}} = 2$ eV, following what was done in Ref. 3), and B1-WC functionals. All approaches highlight the existence of two distinct ferrimagnetic phases, sharing the same total magnetic moment of $2\mu_B$ per cell, but with distinct local magnetic moments:[20] while the Cr^{3+} cations always remain in their usual high-spin state, the Fe^{3+} cations can be either in a high-spin (HS) or low-spin (LS) state. For brevity, in the following we refer to these two cases as the "FiMHS phase" and "FiMLS phase," respectively. The local magnetic moments, together with the respective structural parameters, are summarized in Table I. All functionals yield very similar structural parameters and magnetic moments. Whatever the approach, the FiMHS phase has a significantly higher volume than the FiMLS phase and a lower energy than the FiMLS phase (and the FM phases). Thus, all considered functionals are in agreement with each other and predict the same HS ground state.

In agreement with our results, the authors of Ref. 3 predicted a FiMHS phase within the LSDA + U (using $U = 3$ eV and $J = 0.8$ eV). Yet, they obtained a FiMLS phase at the LSDA level. Our investigations suggest that their LSDA result is in fact a local minimum rather than the true LSDA ground state. We are convinced that their calculations were performed very thoroughly, but the electronic structure of this family of materials is so complex that many different competing magnetic states, with comparable energies, coexist. The fact that calculations based on different functionals, basis sets (PAW, Gaussian) and codes (VASP and CRYSTAL) yield similar results is a strong indication that the existence of FiMHS and FiMLS phases is not a numerical artifact but an intrinsic property of this material, and probably typical of the $Bi_2MM'O_6$ family. Our B1-WC results, which do not involve the adjustment of semiempirical parameters, strengthen this conclusion.

In order to quantify the magnetic interactions within each of these phases, we have also considered ferromagnetic configurations. Full relaxations within the LSDA + U ($U = 3$ eV and $J = 0.8$ eV) and B1-WC yield ferromagnetic FMLS and FMHS phases with respective total magnetic moments of $4\mu_B$ and $8\mu_B$. Essentially, they are linked to their ferrimagnetic counterparts through an inversion of the Fe spin as they share nearly identical structural parameters and absolute values of the local magnetic moments. Note that the energy difference between the FiM and FM states is significantly larger when we have HS-Fe^{3+}, indicating weaker exchange interactions in the LS case. This is consistent with the fact that, in the LS phases, only Fe^{3+} t_{2g} orbitals are occupied, and such orbitals are usually rather localized compared with their e_g counterparts.

B. Electronic properties

We then further characterized the electronic properties of the FiMHS, FiMLS, FMHS, and FMLS phases by

TABLE I. Summary of the structural and electronic properties of the FiMHS-Fe and FiMLS-Fe phases of Bi_2FeCrO_6 as computed using different functionals. a and α are the rhombohedral cell parameters, Ω the unit cell volume, x_i, y_i and z_i denote the Wyckoff positions of the *R3* spacegroup occupied by the atoms in the unit cell. μ_{Fe} and μ_{Cr} are the local magnetic moments. The last line indicates the character (HM = half-metal, I = insulator) of each phase and is based on the DOS calculations presented in Sec. III B. In brackets we indicate the results of Baettig *et al.* (Ref. 3) for the FiMHS-Fe phase that they relaxed using the LSDA + U with $U = 3$ eV and $J = 0.8$ eV. ΔE is, for each of the functionals, the energy difference between the corresponding phase and the FiMHS ground state.

Functional	LSDA		LSDA + U $U_{\text{eff}} = 2$ eV		LSDA + U $U = 3$ eV, $J = 0.8$ eV				B1-WC			
Phase	FiMHS	FiMLS	FiMHS	FiMLS	FiMHS	FiMLS	FMHS	FMLS	FiMHS	FiMLS	FMHS	FMLS
a in Å	5.47	5.33	5.49	5.38	5.48 (5.47)	5.37	5.49	5.37	5.57	5.43	5.58	5.43
α in °	60.16	60.99	60.04	60.68	60.04 (60.09)	60.80	60.04	60.78	59.54	60.23	59.46	60.29
Ω in Å^3	116.08	109.57	116.82	111.72	116.57(116.86)	111.33	117.18	111.64	120.61	114.00	121.11	114.20
x_{Bi}	0.000	0.000	0.000	0.000	0.000 (0.000)	0.000	0.000	0.000	0.000	0.000	0.000	0.000
x_{Bi}	0.504	0.499	0.503	0.499	0.503(0.503)	0.500	0.504	0.499	0.503	0.499	0.504	0.500
x_{Fe}	0.734	0.731	0.732	0.729	0.732 (0.732)	0.730	0.731	0.731	0.724	0.721	0.723	0.722
x_{Cr}	0.226	0.234	0.225	0.231	0.226(0.226)	0.232	0.226	0.232	0.217	0.223	0.216	0.223
x_{O1}	0.539	0.548	0.544	0.549	0.544 (0.545)	0.550	0.546	0.550	0.516	0.523	0.516	0.524
y_{O1}	0.955	0.957	0.950	0.953	0.950(0.950)	0.956	0.949	0.953	0.933	0.939	0.933	0.938
z_{O1}	0.394	0.417	0.396	0.415	0.398 (0.398)	0.414	0.400	0.413	0.407	0.421	0.410	0.420
x_{O2}	0.050	0.044	0.047	0.043	0.047(0.047)	0.046	0.044	0.045	0.017	0.018	0.014	0.019
y_{O2}	0.907	0.912	0.905	0.907	0.905 (0.905)	0.908	0.905	0.908	0.914	0.914	0.915	0.913
z_{O2}	0.444	0.460	0.446	0.460	0.447(0.448)	0.461	0.449	0.457	0.431	0.443	0.432	0.442
μ_{Fe} in μ_B	−3.65	−0.60	−3.96	−0.87	−3.99 (−4.00)	−0.86	4.04	1.02	−4.22	−0.98	4.23	1.04
μ_{Cr} in μ_B	+2.14	+2.43	+2.57	+2.75	+2.55 (+2.50)	+2.75	2.86	2.73	+2.82	+2.90	2.99	2.90
Character	HM	HM	I	I	I	I	I	I	I	I	I	I
ΔE in meV	0	535	0	468	0	382	164(176)	404	0	1083	64	1078

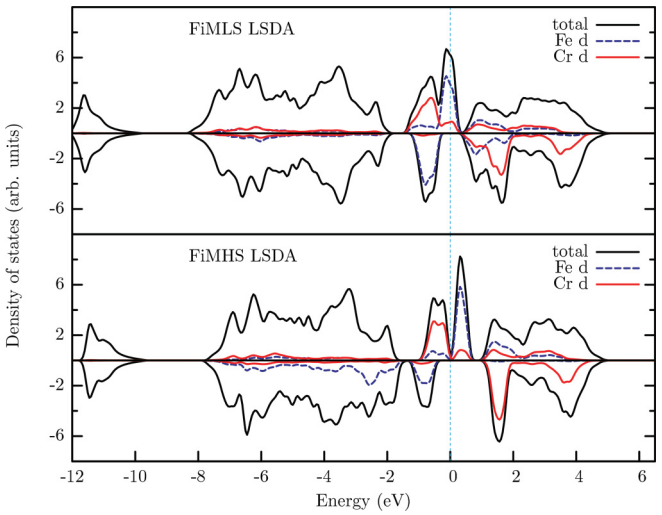

FIG. 1. (Color online) Projected DOS of the FiMHS and FiMLS phases of Bi_2FeCrO_6 obtained within within the LSDA.

analyzing the partial DOS of each of the previously identified (meta)stable structures. In Fig. 1 we show our results obtained within the LSDA and in Figs. 2 and 3 we respectively show the four phases (FiMHS, FiMLS, FMHS, and FMLS) within the LSDA + U (with $U = 3$ eV and $J = 0.8$ eV) and B1-WC. The LSDA + U results are very similar to those obtained with $U_{\text{eff}} = 2$ eV so we will not show the latter ones.

We notice that our LSDA and LSDA + U results are not directly comparable to those presented by Baettig *et al.*,[3] because they do not refer to the same structures: in order to isolate structural and electronic effects, these authors kept the structure of the LSDA FiMLS phase and computed the DOS using different functionals, while we performed full relaxations in each case. Nevertheless, our FiMHS results for the LSDA + U functional with $U = 3$ eV and $J = 0.8$ eV closely resemble the DOS shown in Ref. 4 for $U = 4$ eV and $J = 0.8$ eV. In order to give a better overview, the insulating (I) or half-metallic (HM) character of each phase has been indicated in Table I.

Just as Baettig *et al.*, we believe that the LSDA does not correctly describe the true character of this material and that more sophisticated approaches are required. We nevertheless want to show these results in order to complete the data they have provided in their paper. For the LS phase, we find a half-metal, but we also find a FiMHS phase which is described in the LSDA as a marginally (half-)metallic state, with a minimum of the DOS at the Fermi level.

The computed electronic structure depends on the choice of the LSDA + U formulation and of the corresponding parameters. For our study we simply used the parameters chosen by Baettig *et al.* to allow a better comparison. To cross-check our results we used the B1-WC hybrid functional. A quick inspection of Figs. 2 and 3 shows a qualitatively very good agreement between both approaches for the total and the projected DOS, for each of the four phases we have considered. Just as in $BiFeO_3$[14] (in this reference electronic band structures rather than DOS are compared), the only notable difference is that B1-WC yields a higher electronic band gap and, in particular, all the phases are predicted to be insulators.

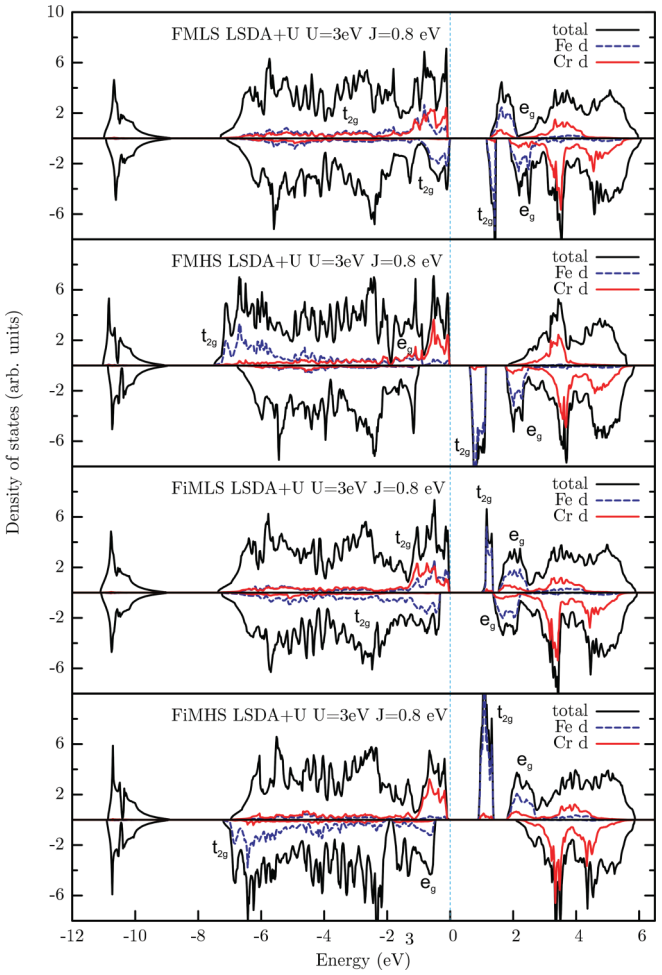

FIG. 2. (Color online) Projected DOS of the FiMHS, FiMLS, FMHS, and FMLS phases of Bi_2FeCrO_6 obtained within the LSDA + U ($U = 3$ and $J = 0.8$ eV). We have performed a qualitative assignment of the Fe-3d t_{2g} and e_g orbitals.

For the FiMHS phase, the band gap is dominated by occupied Cr-3d and empty Fe-3d states. As regards the iron states, our results indicate they are significantly hybridized with the O-2p states: they extend throughout the energy range of the valence band, peaking at the band bottom. For the FiMLS phase, the band gap is characterized by occupied Cr-3d states and occupied and unoccupied LS-Fe orbitals. It can be seen that LS and HS phases are characterized by very different splittings between Fe-d t_{2g} and e_g orbitals, which suggests that the Fe atoms experience a larger crystal field in the LS phase. This will be further discussed in Sec. III C.

Except for the expected spin flippings resulting from the different magnetic ordering, the DOS of the FM phases are very similar to the FiM phases, which is consistent with the structural similarities pointed out earlier.

C. Pressure-induced spin crossover

Since we highlighted the existence of four different phases, we now investigate their relative stability. As discussed earlier, the HS phases (FiM and FM) have a significantly higher volume than the LS phases, and in Fig. 4 we plot, for the LSDA + U (with $U = 3$ eV and $J = 0.8$ eV) and B1-WC, the

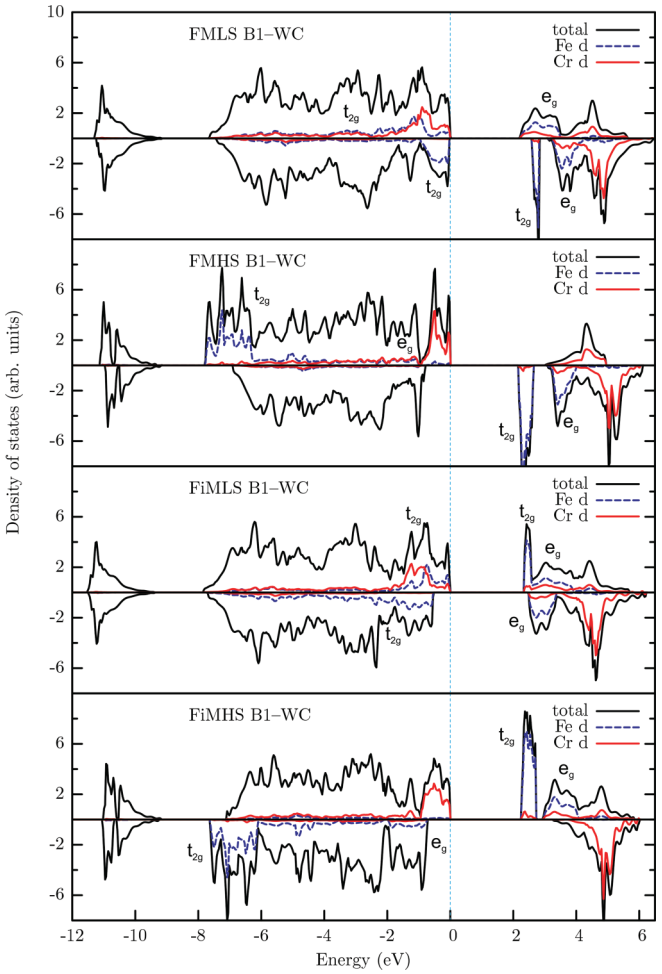

FIG. 3. (Color online) Projected DOS of the FiMHS, FiMLS, FMHS, and FMLS phases of Bi_2FeCrO_6 obtained within B1-WC. We have performed a qualitative assignment of the Fe-3d t_{2g} and e_g orbitals.

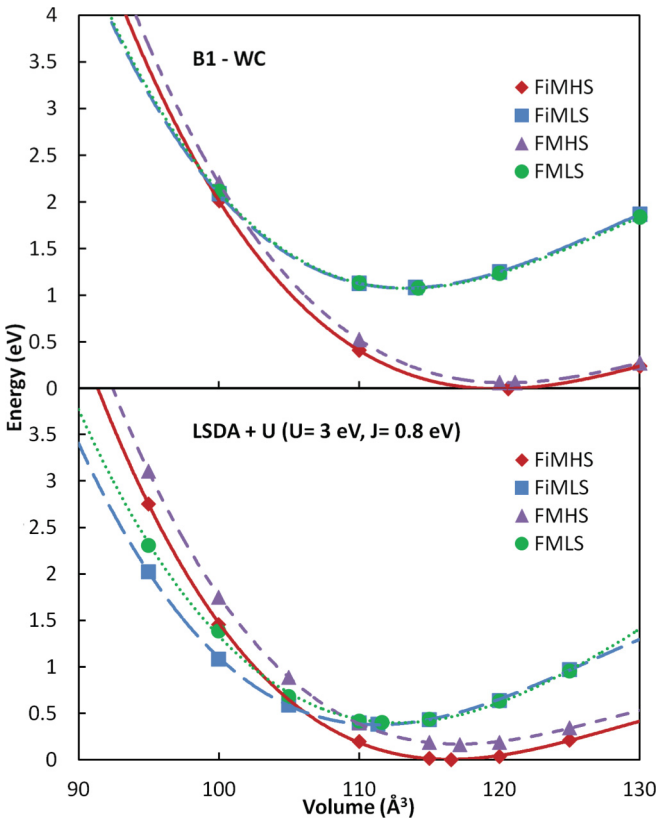

FIG. 4. (Color online) Energy versus volume plot for the FiMHS (diamonds, red solid line), FiMLS (squares, blue long dashes), FMHS (triangles, purple short dashes) and FMLS (circles, green dotted line) phases of Bi_2FeCrO_6, as obtained within the LSDA + U ($U = 3$ eV and $J = 0.8$ eV), and B1-WC.

energy of each phase in terms of the volume, together with the corresponding curve fits.

First, we observe that the global energy minimum in each case corresponds to the FiMHS phase, showing that all functionals coherently predict a FiMHS ground state. The structurally very similar FMHS phase is also energetically quite close to the FiMHS phase. Both LS phases have not only a significantly lower equilibrium volume but a much higher energy. As mentioned above, for the LS phases the energy difference between FiM and FM states is smaller than for the HS phases. The LSDA + U seems to predict that the FiMLS phase is more stable than the FMLS phase at lower volume, but for B1-WC we cannot reliably predict which of the phases is the most stable, as the corresponding curves nearly coincide. In case the transition is to the FMLS phase it would be also accompanied with a significant change of the total magnetic moment (from $2\mu_B$ in the FiMHS phase to $4\mu_B$ in the FMLS phase).

However, it is very interesting to notice that, independently of the functional, both groups (LS and HS) of fitted curves cross, indicating a change of the relative stability of the HS and LS phases at a given volume. At larger volumes, the HS structure is the most stable, while at lower volumes the LS structure becomes more stable. This behavior indicates the possibility of a strain or pressure-induced phase transition from the FiMHS ground state to a FiMLS or maybe FMLS structure. We have also estimated the critical transition pressure predicted by each functional via the slope of the common tangent of the fitted curves (For LSDA and LSDA + U with $U_{\text{eff}} = 2$ eV, similar plots for FiM phases have been obtained but are not shown here). The results are given in Table II.

The value of the transition pressure is very dependent on the functional and in particular the choice of U and J, but all functionals agree on the existence of such a transition. Interestingly,

TABLE II. Critical transition pressure estimated via the slope of the common tangent for different functionals.

Functional	LSDA	LSDA + U ($U_{\text{eff}} = 2$ eV)	LSDA + U ($U = 3$ eV, $J = 0.8$ eV)	B1-WC
p_c (GPa)	1.71	19.61	13.61	35.49

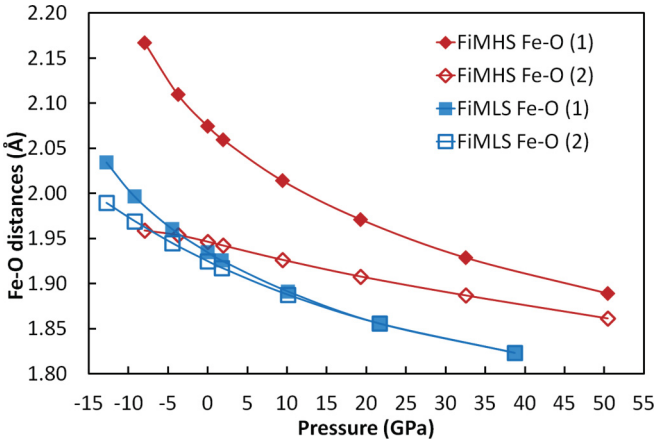

FIG. 5. (Color online) Fe-O distance versus pressure plot for the FiMHS (red diamonds) and FiMLS (blue squares) phases of Bi_2FeCrO_6, as obtained within LSDA + U ($U = 3$ eV and $J = 0.8$ eV). Full symbols correspond to the first set of O atoms, empty symbols to the second set.

our hybrid calculations place the transition pressure at about 35 GPa, in significant agreement with what has been obtained for $BiFeO_3$ both experimentally[6] and computationally using an LSDA + U approach with $U_{\text{eff}} = 3$ eV.[5] Hence, our results add to the evidence that Fe^{3+} undergoes a HS to LS transition at about 35 GPa in $BiFeO_3$ and related compounds.

While the HS phase is favored by Hund's rule, the LS phase might result from a larger splitting of t_{2g} and e_g orbitals arising from a larger crystal field, as suggested at the end of the previous section. In order to provide support for this argument, we now compare the Fe-O distances in the FeO_6 octahedra of the FiMHS and FiMLS phases, as obtained within LSDA + U ($U = 3$ eV and $J = 0.8$ eV). Figure 5 shows how they evolve with pressure. As the structures present two nonequivalent sets of O atoms, we report two Fe-O distances for each phase and pressure. Also, as the corresponding FM phases are nearly isostructural (see Table I) the following discussion remains valid for them too. For the relaxed FiMHS ground state (i.e., at zero applied pressure), the Fe-O distances equal 2.075 and 1.946 Å. In the fully relaxed FiMLS structure, these distances become 1.925 and 1.935 Å. It can be clearly appreciated that, in the whole pressure range, the Fe-O distances are significantly smaller for the LS phase, the difference being of the order of 0.05–0.10 Å. This is fully compatible with the stronger crystal field expected in the LS structure. Additionally, we notice that the Fe atoms in the LS phase stay almost at the center of the O_6 octahedron, while they significantly displace off-center in the HS structure. This concomitant reduction of the ferroelectric distortion associated with Fe when moving from the HS to the LS configuration had already been observed to occur in high-pressure phases of $BiFeO_3$ that present Fe^{3+} in the LS configuration (Ref. 5) and is again found here. These modifications of the atomic configuration justify the significantly smaller volume of the LS phase, which can, in turn, explain its stabilization at high pressure.

IV. CONCLUSIONS

First we have shown that Bi_2FeCrO_6 presents four competing phases with distinct electronic and magnetic properties. Two of the phases are ferrimagnetic and have the same total magnetic moment of $2\mu_B$ per unit cell, but differ in the electronic configuration of the Fe^{3+} cations, which present high-spin (FiMHS-Fe) and low-spin (FiMLS-Fe) states, respectively. The other two phases are ferromagnetic and have a total magnetic moment of $4\mu_B$ (FMLS) and $8\mu_B$ (FMHS) per unit cell, respectively. These results have been checked using the LSDA approach, different LSDA + U variants, and the hybrid functional B1-WC; each of these functionals predicted that the FiMHS-Fe phase is the ground state at ambient conditions. Next, considering our DOS calculations and the work of Baettig *et al.*, there is no doubt that this ground-state phase is insulating and our new calculations indicate that the other three phases are also insulating. Finally, we have shown that all the functionals predict a pressure-induced transition from the FiMHS-Fe to a LS-Fe phase. Depending on the actual energy of the FiMLS and FMLS phases, this might be even a transition phase with a change of the total magnetic moment. Together with previous works on $BiFeO_3$, our study suggests that other members of the $Bi_2MM'O_6$ family may present similar properties and therefore deserve extended research interest. In particular, detailed experimental studies would be needed to identify and validate first-principles methods for quantitatively accurate simulations of these systems, and to open up perspectives for fully predictive calculations in this complex and interesting class of materials.

ACKNOWLEDGMENTS

This work was supported by MaCoMuFi and OxIDes European projects, by the European Multifunctional Materials Institute (EMMI) and by the Interuniversity Attraction Poles Program (Grant No. P6/42), Belgian State-Belgian Science Policy. J.I. thanks financial support from MICINN-Spain (Grants No. MAT2010-18113, No. MAT2010-10093-E, and No. CSD2007-00041). Ph.G. acknowledges the Francqui Foundation.

[1]R. Nechache, C. Harnagea, A. Pignolet, F. Normandin, T. Veres, L.-P. Carignan, and D. Menard, Appl. Phys. Lett. **89**, 102902 (2006).
[2]R. Nechache, C. Harnagea, L.-P. Carignan, O. Gautreau, L. Pintilie, M. P. Singh, D. Menard, P. Fournier, M. Alexe, and A. Pignolet, J. Appl. Phys. **105**, 061621 (2009).
[3]P. Baettig, C. Ederer, and N. A. Spaldin, Phys. Rev. B **72**, 214105 (2005).
[4]P. Baettig and N. A. Spaldin, Appl. Phys. Lett. **86**, 012505 (2005).
[5]O. E. González-Vázquez and J. Íñiguez, Phys. Rev. B **79**, 064102 (2009).

[6]A. G. Gavriliuk, V. V. Struzhkin, I. S. Lyubutin, S. G. Ovchinnikov, M. Y. Hu, and P. Chow, Phys. Rev. B **77**, 155112 (2008).
[7]S. Speziale, A. Milner, V. E. Lee, S. M. Clark, M. P. Pasternak, and R. Jeanloz, Proc. Natl. Acad. Sci. **102**, 17918 (2005), and references therein.
[8]G. Kresse and J. Furthmüller, Phys. Rev. B **54**, 11169 (1996).
[9]G. Kresse and J. Furthmüller, Comput. Math. Sci. **6**, 15 (1996).
[10]G. Kresse and J. Hafner, Phys. Rev. B **47**, 558 (1993).
[11]S. L. Dudarev, G. A. Botton, S. Y. Savrasov, C. J. Humphreys, and A. P. Sutton, Phys. Rev. B **57**, 1505 (1998).
[12]V. I. Anisimov, F. Aryasetiawan, and A. I. Liechtenstein, J. Phys.: Condens. Matter **9**, 767 (1997).
[13]D. I. Bilc, R. Orlando, R. Shaltaf, G.-M. Rignanese, J. Íñiguez, and Ph. Ghosez, Phys. Rev. B **77**, 165107 (2008).
[14]M. Goffinet, P. Hermet, D. I. Bilc, and Ph. Ghosez, Phys. Rev. B **79**, 014403 (2009).
[15]R. Dovesi, V. R. Saunders, C. Roetti, R. Orlando, C. M. Zicovich-Wilson, F. Pascale, B. Civalleri, K. Doll, N. M. Harrison, I. J. Bush, Ph. D'Arco, and M. Llunell, CRYSTAL06 User's Manual, University of Torino, 2006 (unpublished).
[16]M. Catti, G. Valerio, and R. Dovesi, Phys. Rev. B **51**, 7441 (1995).
[17]M. Catti, G. Sandrone, G. Valerio, and R. Dovesi, J. Phys. Chem. Solids **57**, 1735 (1996).
[18]S. Pikunov, E. Heifets, R. I. Eglitis, and G. Borstel, Comput. Mater. Sci. **29**, 165 (2004).
[19]W. R. Wadt and P. J. Hay, J. Chem. Phys. **82**, 284 (1985).
[20]Local magnetic moments were obtained by integration within a sphere for LSDA and LSDA + U calculations and Mulliken population analysis for B1-WC calculations.